Development of a zero-dimensional model and application on a medium-speed marine four-stoke diesel engine.

Miltiadis Kalikatzarakis[a*], Andrea Coraddu[a], Gerasimos Theotokatos[a] and Luca Oneto[b]

[a] Naval Architecture, Ocean & Marine Engineering, University of Strathclyde, Glasgow, UK
[b] DIBRIS, University of Genova, Genova, Italy
* Miltiadis.kalikatzarakis@strath.ac.uk

Abstract

The present study deals with the development of a zero-dimensional model for marine diesel engines of the four-stroke type, as well as a methodology to automate its calibration process. The modelling and calibration approach is validated using experimental and operational data from a Warstila engine, covering several model input and outputs. Validation results suggest that the modelling approach suggested, can predict the stationary and transient responses of the engine within 3.5% on measurements taken during the vessel's operation for a variety of loads ranging between 20% to 100%, with minimal calibration effort from the modeller.

Keywords: zero-dimensional model, dynamic simulation, parameter estimation, model validation

1 INTRODUCTION

In recent years, the maritime industry is confronted by several challenges, including volatile bunker prices that affect cargo transportation costs and the shipowners' competitiveness and viability of their operations [1], and strict regulations to limit emissions and their environmental impact, with the aim of reducing CO_2 emissions from shipping by 40-50% [2 – 4]. As a result of this combination, energy efficiency and environmental sustainability of maritime operations is currently prioritized in the maritime industry. Shipowners and operators are adopting measures to lower fuel consumption and associated emissions, and researchers in the are researching innovative technologies and methods that can increase the environmental efficiency and cost-effectiveness of ship operations.

Improvements in energy efficiency can be obtained in a variety of design and retrofit measures, such as hull design optimization, adoption of alternative fuels, and alternative energy sources [5 – 7], as well as operational measures, including speed optimisation, better capacity utilisation and advanced route planning execution methods [8 – 12]. Regardless of the proposed approach, it is widely known that for most of the vessels operating today, the main engines, and to a lesser extent the auxiliary engines, are the main factors of energy loss on-board [13 – 14]. For this reason, engine manufacturers have also introduced a variety of technologies to improve operational efficiency and emission reduction, with ongoing development work concentrating on reducing fuel consumption, utilising alternative fuels, as well as further increasing diesel engine (DE) power density and enhancing operating performance [15].

Nevertheless, the identification and adoption of innovative and emerging technologies in marine DEs is limited by the expensive design, prototyping and experimentation processes [14 – 16]. To mitigate this issue, various computer modelling approaches have been developed to represent the physical processes that occur in a DE under steady-state and transient conditions, as a means of a rapid and cost-effective prototyping tool. Depending on the application requirements, mathematical representations of a varying range of accuracy and computational complexity are available in the literature. Most widely employed are Mean Value Engine Models (MVEMs) [17 – 24], which provide adequate accuracy in the prediction of most engine parameters while being computationally cheap, and zero-dimensional (0D models) that operate on per per-crank basis, allowing the calculation of parameters of the gas within the engine cylinders [25 - 30]. Finally, several attempts to combine both approaches have also been proposed and utilised in a variety of applications, reportedly surpassing the predictive abilities of MVEMs with lower computational requirements than their 0D counterparts [31 - 34].

Common in these studies is the interest in improving and certifying the credibility and accuracy of the developed mathematical model. As such, the model verification, calibration, and validation processes occupy a central role, based on which the predictive capabilities of the model are assessed to justify its use for the application of interest. In this respect, our main objective is to develop a model for a marine DE of the four-stroke type, and a computationally efficient optimisation-based framework for automatic calibration that can reduce the setup time of similar modelling approaches, which is a common issue encountered by engineers and researchers in the field. The validation of the approach is finally demonstrated on a set of operational data from a

turbocharged, four-stroke medium-speed DE of a Roll-on / Roll-off vessel.

The rest of the paper is organised as follows. Section 2 gives a detailed description of the mathematical model developed. Section 3 describes the calibration procedure employed to identify suitable parameter values for the case study engine. Section 4 gives an overview of the data utilised to calibrate and validate the modelling approach, and Section 5 discusses the performance of the model. Finally, conclusions are drawn in Section 6.

Table 1. Acronyms.

Acronym	*Description*
BMEP	Break Mean Effective Pressure
DE	Diesel Engine
LHV	Lower Heating Value
MVEM	Mean Value Engine Model
MCR	Maximum Continuous Rating
ST	Shop Trials
TC	Turbocharger
0D	Zero-Dimensional
MAPE	Mean Absolute Percentage Error
MAE	Mean Absolute Error
PPMCC	Pearson Product-Moment Correlation Coefficient

2 NUMERICAL MODEL

As a case study we have utilised the Warstila 6L46, four-stoke DE. It contains 6 cylinders with 0.46 m bore and 0.58 m stroke, with a Maximum Continuous Rating (MCR) of 5.43 MW at 500 rpm, and two turbochargers (TCs) operating in parallel to deliver the necessary air. The primary characteristics and layout of the engine are presented in Table 2 and Figure 1, which also contains the model states.

Table 2. Main Characteristics of the case study engine.

Model	Wartsila 6L46
Bore Diameter	460 mm
Stroke Length	580 mm
Number of Cylinders	6
Revolutions per Cycle	2
Engine Speed at MCR	500 rpm
Brake Power at MCR	5430 kW

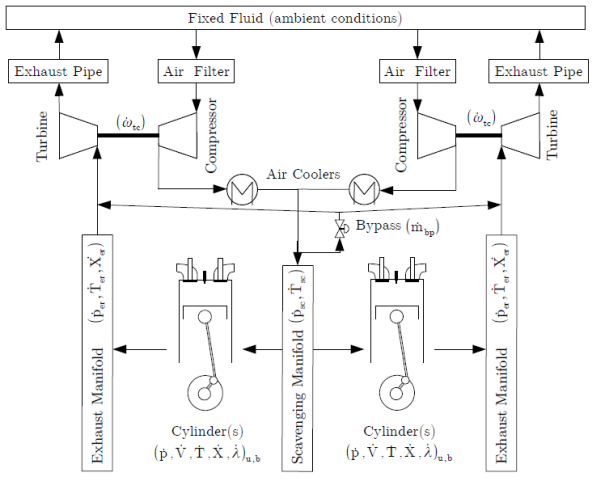

Figure 1. Layout of the modelled engine with all relevant components and model states.

The engine scavenging air and exhaust gas receivers are modelled as control volumes, whereas the compressor and turbine are modelled as flow elements. The exhaust receiver contains states for pressure (p), temperature (T) and exhaust gas composition (X), whereas the gas composition for the air path has been assumed constant. The engine boundaries are modelled using fixed fluid elements of constant pressure and temperature, and shaft elements are utilised to compute the rotational speed of the turbocharger (ω_{tc}) and crankshaft (ω_e). Finally for the in-cylinder process we utilised a two-zone 0-D approach, with state quantities being the in-cylinder pressure, temperature, gas composition and air-fuel equivalence ratio (λ) for each zone. The governing equations of all relevant components will be discussed in Sections 2.1 - 2.6.

2.1 Gas Composition and properties

The working fluid of the engine is considered to be a mixture of the following 11 species: CO_2, H_2O, N_2, O_2, CO, H_2, O, H, OH, NO and N. The thermodynamic properties of the gas are calculated using the NASA polynomials [35], under the assumption of a thermally perfect gas. The concentration along the air path is assumed constant and equal to the standard air concentration.

2.2 Control Volumes

The control volumes are modelled using the open thermodynamic system concept [36 – 37], and use as inputs the pressure, temperature, and composition of the working medium contained in the adjacent elements.

Considering the control volumes as cylindrical solenoids, neglecting dissociation effects and the kinetic energy of the flows entering / exiting the receivers, and assuming ideal gas, the change of rate in the mass stored in the volume can be derived from the mass conservation law, the temperature rate of change is derived from the energy conservation law, and the pressure of the working medium can be computed using the ideal gas law equation as

$$\frac{dm}{dt} = \sum_i \dot{m}_{in,i} - \sum_j \dot{m}_{out,j} \tag{1}$$

$$\frac{dT}{dt} = \frac{\dot{Q} + \sum_i (mh)_{in,i} - \sum_j (mh)_{out,j} - u\frac{dm}{dt}}{mc_v} \tag{2}$$

$$\frac{dp}{dt} = \frac{R}{V}\left(T\frac{dm}{dt} + m\frac{dT}{dt}\right) \tag{3}$$

where m_i is the mass flow rate of stream i and the subscripts in, out refer to flows entering and exiting the control volume, respectively. mh refers to the enthalpy flow rate, and $\dot{Q} = kA(T - T_{amb})$ represents the heat transfer from the control volume to the surrounding environment, with k being the heat transfer coefficient, computed according to [38], and A being the heat transfer area.

Moreover, considering the control volume as a well-stirred mixer, the dynamics of the concentration states can be derived as [39]

$$\frac{dX}{dt} = \frac{RT}{pV}\sum_j \left(X_{in,j} - X\right)\dot{m}_{in,j} \quad (4)$$

where $R = R(X,T)$ is the gas mixture constant.

2.3 Valves

The mass flow rate through a valve is computed assuming subsonic flow through a flow restriction [37], with the valve opening signal (lift) as input.

The bypass valve is assumed to be activated if the pressure on the compressor exceeds 90% of the surge limit for the instantaneous flow rate. Furthermore, we have assumed a linear opening characteristic, with the reference area considered as a calibration parameter. For the intake and exhaust valves, we utilised a non-linear characteristic, parameterised on the maximum crossflow area of the inlet and exhaust valved, and crank-angle duration that the valve stays at its maximum lift [38].

2.4 Air Cooler, air filter, exhaust pipes

Pressure losses in all these components, as well as air cooler effectiveness (ϵ_{ac}), have been modelled as quadratic functions of their corresponding input mass flow rate, and the temperature at the air cooler outlet is given by

$$T_{ac}^{out} = \epsilon_{ac} T_w + (1 - \epsilon_{ac}) T_{ac}^{in} \quad (5)$$

with T_w being the temperature of the cooling water.

2.5 Turbochargers

The engine has two turbocharging units operating in parallel to supply the engine with sufficient air mass flow. We modelled the compressor using its steady state performance map, which provides the relations between the compressor performance variables: reference flow rate, pressure ratio, reference speed and isentropic efficiency.

The rotational speed and pressure ratio are considered as inputs to the model, which allows the computation of the reference flow rate and isentropic efficiency through interpolation [14, 40]. The temperature at the outlet of the compressor is given by [36]

$$T_c^{out} = T_c^{in}\left(1 + \frac{\Pi_c^{\frac{\gamma-1}{\gamma}} - 1}{\eta_c}\right) \quad (6)$$

where Π_c is the pressure ratio of the compressor, corrected for the pressure losses in the air cooler and air filter.

For the turbine, we utilized its swallowing capacity and efficiency maps, which allow the calculation of the turbine flow rate and isentropic efficiency through interpolation, with the turbine pressure ratio Π_t corrected for the exhaust pipe pressure losses. The temperature at the turbine outlet is computed through the turbine isentropic efficiency (η_t) definition as

$$T_t^{out} = T_t^{in}\eta_t\left(1 - \Pi_t^{\frac{\gamma-1}{\gamma}}\right) \quad (7)$$

with γ being the ratio of specific heats of the medium.

The rotational speed of the turbochargers is a model state, defined by the power balance between compressor and turbocharger as

$$\frac{d\omega_{tc}}{dt} = \frac{P_t\eta_{tc}^{mech} - P_c}{J_{tc}\omega_{tc}} \quad (8)$$

where P_c, P_t refer to the turbine and compressor power, respectively, and J_{tc} refers to the turbocharger shaft inertia. Finally, η_{tc}^{mech} corresponds to the mechanical efficiency of the turbocharger unit, accounting for friction losses.

2.6 Cylinders

For the in-cylinder process, apart from the assumptions underlined in Section 2.1 regarding the working medium we have further neglected valve leakage and blow-by. Furthermore, the temperatures at the cylinder wall, head, piston wall, liner wall, exhaust valve wall, as well as the injected fuel temperature are all uniform and constant, as the temperature variations of the inner cylinder surface during the thermodynamic cycle are weak compare to the temperature variations of the combustion gases [41, 42].

Moreover, we have assumed uniform cylinder pressure, and that the combustion chamber is composed of two combustion zones, the burned zone containing incompletely oxidized fuel denoted with the subscript (b), and unburned zone containing air and fuel, referred to with the subscript (u). Each zone is spatially homogeneous, separated by an infinitesimally thin flame without mass, and no heat transfer between the two zones. A schematic is presented in Figure 2.

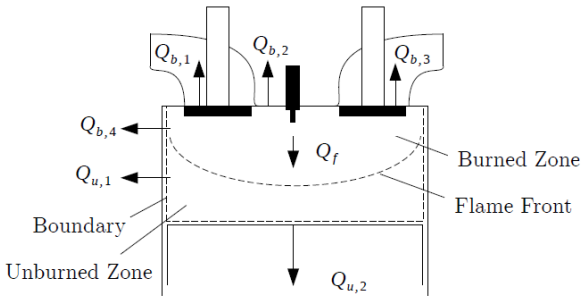

Figure 2. Energy flow of the two – zone combustion model.

The main equations governing the model include the conservation of mass and energy, and the equations of state of the working medium and the evolution of volume in each zone, as

$$\frac{dm}{d\theta} = \frac{dm_u}{d\theta} + \frac{dm_b}{d\theta} = \frac{dm_f}{d\theta} + \frac{dm_a}{d\theta} \quad (9)$$

$$\frac{d(m_u u_u)}{d\theta} = -p\frac{dV_u}{d\theta} - \sum_i \frac{dQ_{u_i}}{d\theta} - h_u \frac{dm_b}{d\theta} \quad (10)$$

$$\frac{d(m_b u_b)}{d\theta} = -p\frac{dV_b}{d\theta} - \sum_i \frac{dQ_{b_i}}{d\theta} + h_u \frac{dm_b}{d\theta} + \frac{dQ_f}{d\theta} \quad (11)$$

$$pV_u = m_u R_u T_u \quad (12)$$

$$pV_b = m_b R_b T_b \quad (13)$$

$$\frac{dV}{d\theta} = \frac{dV_u}{d\theta} + \frac{dV_b}{d\theta} \quad (14)$$

where the subscripts (a, f) refer to air and fuel, θ refers to the crank angle, $\sum_i \frac{dQ_i}{d\theta}$ refers to the summation of heat transfer rates through the engine's different parts' surfaces in contact with the cylinder gases, and $\frac{dQ_f}{d\theta}$ refers to the heat release rate.

We have utilised a double Wiebe profile for the heat release rate, to account for the premixed and diffusive combustion processes [38, 43, 44]. While the Wiebe functions by no means describe the complex fuel air mixing in the diesel combustion process, they can provide valuable thermodynamic input for the model in terms of a realistic (shape of the) heat release. The Wiebe profile was calibrated at the nominal point of the engine, and we have estimated the ignition delay according to Sitkey [45]. The heat transfer between the mass trapped in the cylinder and the surrounding areas is calculated according to the standard Newtonian relation, with the heat transfer coefficient evaluated according to [48]. The friction mean effective pressure is evaluated according to [49], as a function of the maximum combustion pressure and engine rotational speed. Finally, the concentration of all combustion products is evaluated utilising the method of [50], under the assumption of chemical equilibrium, except for thermal NO_X which is computed according to the extended Zeldovich mechanism [51].

2.7 Sensor Dynamics

The thermal inertia of the temperature sensors (s), which are mounted on the outer surface of the exhaust pipes, is modelled as a first-order system [39]

$$\frac{\mathrm{dT_s}}{\mathrm{dt}} = \frac{\mathrm{T} - \mathrm{T_s}}{\tau_s} \quad (15)$$

where T_s refers to the temperature including the sensor dynamics, and T is the temperature of the working medium in the engine. The time constant τ_s is considered as a calibration parameter. Dynamic response for all other sensors has been neglected, as it is known to be in the order of milliseconds [52].

2.8 Calculation Procedure

Inputs towards the cylinder model include the pressure, temperature and medium composition from the scavenging manifold, the pressure of the exhaust manifold, engine rotational speed and fuel injected per cycle from the governor. Subsequently, the cylinders air and exhaust gas mass flow rates, pressures, temperatures, the composition of the exhaust gas, and the equivalence ratio of the exhaust gas exiting the cylinders are calculated. Additional outputs include the energy flow of the exhaust gas exiting cylinders, the indicated power, the friction power, brake power torque, brake specific fuel consumption and engine brake efficiency.

For all the other components, being split either control volumes or flow elements, the following structure is employed: Inputs required for the flow elements are utilised from the adjacent flow receiver, or fixed fluid structures for the engine boundaries, which include the necessary parameters to fully characterise the working medium state (temperature, pressure, composition). Subsequently, mass and energy flows through the flow elements are computed and provided to the adjacent control volumes. In addition, the absorbed compressor torque and produced turbine torque are calculated and are used as inputs to the turbocharger shaft element, which derives the turbocharger speed, which, in turn, is provided to the turbine and compressor blocks.

This framework forms an additional system of first order differential equations, that is solved for each time step by using the classic Runge-Kutta method. In total, the model contains 50 states over two major integration steps.

Parameters include the geometric data of the engine, the intake and exhaust valves profiles, the compressor and turbine performance maps, the bypass valve geometric and control details, constants present in any sub-model, and the ambient conditions for the engine boundaries. Finally, initial values are also required for the engine and turbocharger rotational speeds, and the temperature, pressure and composition of the working medium contained in the scavenging and exhaust manifolds.

3 MODEL PARAMETERISATION

The proposed model contains internal feedback systems, hence the modelling errors of any subsystems will be propagated and amplified towards the rest of the model. As such, balancing out the complete model by readjusting the model parameters is essential to obtain an overall accurate model [39].

The calibration process is treated as an optimisation problem, with the objective being to minimise the error between the model estimated outputs and the available measurements. This is performed in two levels, or sub-problems: the calibration of the parameters that affect the performance of the model in stationary conditions, referred to as Problem 1 ($\mathcal{P}_1$), and the calibration of the parameters that affect the dynamic behaviour of the model, referred to as Problem 2 ($\mathcal{P}_2$).

3.1 Optimisation Problem Formulation

Formally, for both problems we seek the solution to the following continuous, non-convex problem:

$$\min_{\phi} \hat{L}(\phi, \mathcal{D}_{\mathcal{M}}) = \sum_{i=1}^{M} l(h(X_i, \phi), y_i) \quad (16)$$
$$\text{subject to: } \phi_{min} \leq \phi \leq \phi_{max}$$

where h refers to the model of Section 2, ϕ is the set of parameters that need to be estimated from a given bounded space Φ, X_i refers to the measurements

corresponding with the model inputs, and y_i refers to the measurements corresponding with the model outputs. $\hat{L}(\phi, \mathcal{D}_{\mathcal{M}})$ is the empirical error of the model h on the dataset $\mathcal{D}_{\mathcal{M}} = \{(X_1, y_1), \dots, (X_M, y_M)\}$, measured according to a loss function $l(h(X, \phi), y)$.

For the loss function we have adopted the absolute relative error, given by

$$l(h(X_i, \theta), y_i) = \sum_{j=1}^{S} \frac{y_i^j - h^j(X_i, \theta)}{y_i^j} \tag{17}$$

Note that, because y is a vector, the loss function of Equation 17 refers to the sum of relative errors of all model outputs $j = (1,2 \dots, S)$ and their corresponding measured values.

3.2 Solution Method

Given the nature of the problem $\mathcal{P}_1$, a Derivative-Free Optimisation (DFO) method must be utilised, as obtaining or estimating the derivatives of the physical models with respect to the parameters is a computationally and time-intensive procedure.

The literature on DFO methods is quite large, with a variety of algorithms that can solve a diverse class of problems [53 – 55]. We have employed an algorithm from the class of directional direct search methods: the mesh-adaptive direct search (MADS) algorithm, which is a local optimisation technique with established convergence theory under certain assumptions [56, 57]. It is essentially an extension of the Generalized Pattern Search algorithm, specifically developed to handle non-smooth, black-box problems [58, 59].

The decision variables for $\mathcal{P}_2$correspond to the turbocharger inertias, control volume sizes and the thermal inertia constants of the temperature sensors. Solving this problem can be complex and requires suitable transient datasets, preferably with the response of the engine on specific acceleration / deceleration manoeuvres. Instead, this procedure is simplified here by setting the values of the control volumes to reasonable values of the real pipe volume sizes based on the engine design drawings and setting the turbocharger inertias to reasonable values based on engines of similar sizes, in a manner similar to [39].

3.3 Performance Metrics

It is important to note that the experimental data needs to be split into two different subsets, to objectively evaluate the performance of h: The set $\mathcal{D}_{\mathcal{M}}$ that is used to tune the parameters of h, and the set $\mathcal{T}_{\mathcal{K}} = \{(X_1^t, y_1^t), \dots, (X_K^t, y_K^t)\}$ to evaluate (test) the performance of h on a real-world scenario. Note that $\mathcal{T}_{\mathcal{K}}$ is required, since the error that h would commit over $\mathcal{D}_{\mathcal{M}}$ would be too optimistically biased, since the latter has been used to estimate h itself.

For this reason, additional performance metrics will be reported in Section 5 that refer separately to the performance of h on $\mathcal{T}_{\mathcal{K}}$ and $\mathcal{D}_{\mathcal{M}}$, in order to provide a complete description of the quality of the model. These metrics include the Mean Absolute Percentage Error (MAPE), computed as the absolute relative loss value of h over a dataset

$$\text{MAPE}(h) = \frac{100}{K} \sum_{i=1}^{N} \left| \frac{y_i^t - h(X_i)}{y_i^t} \right| \tag{18}$$

the Mean Absolute Error (MAE), computed as the absolute loss of h

$$\text{MAE}(h) = \frac{1}{N} \sum_{i=1}^{N} |y_i - h(X_i)| \tag{19}$$

and the Pearson Product-Moment Correlation Coefficient (PPMCC), which measures the linear dependency between $h(X_i)$ and y_i with $i \in \{1, 2, \dots, M\}$, given by

$$\text{PPMCC}(h) = \frac{\sum_{i=1}^{N} (y_i - \bar{Y}) \left(h(X_i) - \hat{\bar{Y}} \right)}{\sqrt{\sum_{i=1}^{N} (y_i - \bar{Y})^2} \sqrt{\sum_{i=1}^{N} \left(h(X_i) - \hat{\bar{Y}} \right)^2}} \tag{20}$$

where $\bar{Y} = \frac{1}{N} \sum_{i=1}^{N} y_i$ and $\hat{\bar{Y}} = \frac{1}{N} \sum_{i=1}^{N} h(X_i)$.

Other state-of-the-art error measures exist, but from a physical point of view the ones already reported give a complete description of the quality of the model, therefore we only report those in Section 5.

4 DATASET DESCRIPTION

The dataset utilized consists of two different data sources: standard (stationary) measurements performed during shop trials (ST) that have been used to calibrate the model ($\mathcal{D}_{\mathcal{M}}$) , and operational data originating from the vessel's data logging system, used by the ship operator for performance monitoring purposes, which have been utilised only to evaluate the performance of the model ($\mathcal{T}_{\mathcal{K}}$) .

Table 3. Measurements available from the engine monitoring system.

Signal	Symbol	Units	Uncertainty
Time stamp	t	-	–
Engine rotational speed	n	rpm	$\pm 0.2\%$
Engine Torque	T	kNm	$\pm 0.8\%$
Fuel consumption	$\dot{m}_f$	kg/sec	$\pm 1.0\%$
Turbocharger rotational speed	n_{tc}	rpm	$\pm 0.2\%$
Charge air temperature at scavenging manifold	$T_{sc,in}$	K	$\pm 1.5\%$
Charge air temperature at compressor outlet	$T_{c,out}$	K	$\pm 1.5\%$
Charge air temperature at compressor inlet	$T_{c,in}$	K	$\pm 1.5\%$
Exhaust gas temperature at turbine outlet	$T_{t,out}$	K	$\pm 1.5\%$

Regarding the operational measurements, these are sampled at 1 Hz for approximately 370 calendar days, which amount to 7900 hours of operation for the case

study engine for a total of 28.5 million data points. We present a summary of the available measurements in Table 3. Furthermore, a qualitative impression of the operating profile covered by the dataset is given in Figure 3.

To identify stationary operations, the dataset was first split into a set of time intervals of continuous operation. Within each interval, operation under stationary conditions is defined as: Any continuous set of measurements for which the rotational speed and load of the engine vary by less than 1%, for a period of at least 3 hours. For each these stationary conditions, the last 10 minutes of measurements were extracted, and the median value of each signal was computed. This allows us to summarise each stationary operation as one value per signal, for a total of K = 256 stationary operation points.

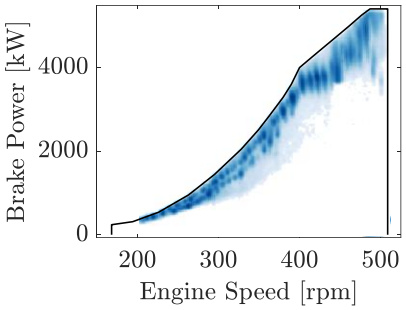

Figure 3. Qualitative view of the operating profile for the case study engine.

5 MODEL VALIDATION

The model is verified by comparing the measured signals of $\mathcal{D}_{\mathcal{M}}$ to the model predictions and validated through comparison with the measured signals of $\mathcal{T}_{\mathcal{K}}$. This process is performed for both stationary and transient conditions. The performance metrics discussed in Section 3.3 are reported in Tables 4, 5 for $\mathcal{D}_{\mathcal{M}}$ and $\mathcal{T}_{\mathcal{K}}$, respectively. A visual impression is presented in Figure 4 for various engine loading conditions.

Table 4. Performance metrics on $\mathcal{D}_{\mathcal{M}}$.

Signal	Units	MAE	MAPE	PPMCC
$p_{c,out}$	Pa	1.2×10^3	0.363	1.000
$p_{t,out}$	Pa	62.354	0.060	1.000
p_{max}	Pa	1.1×10^5	0.981	0.999
$T_{c,out}$	K	2.750	0.638	1.000
$T_{sc,in}$	K	0.393	0.122	0.979
$T_{t,out}$	K	0.066	0.010	1.000
n_{tc}	Hz	4.302	0.041	0.989
sfc	g/kWh	1.207	0.056	0.988
$BMEP$	Pa	1.8×10^4	0.122	1.000

Considering the verification process i.e., the performance of the model on $\mathcal{D}_{\mathcal{M}}$, Table 4 indicates that the model can capture all measurements well within 1% for engine loads ranging between 20% - 100%. The highest errors appear for the maximum combustion pressure, with a MAPE equal to 0.981%, which amounts to a deviation of 1.2×10^5 Pa. The lowest discrepancy between the model and the measurements is reported for the temperature on the turbine outlet, with a MAPE of only 0.01%, or 0.06 K, well within the uncertainty of most conventional thermocouples used for this application. The prediction accuracy on all other variables is equally good, regardless of the subsystem considered. Although not shown for the sake of brevity, the highest deviation for all measured signals appears for loads equal to 20% of the maximum rated power. This is of course not desirable, but the engine is very rarely operating at low loads for prolonged periods of time.

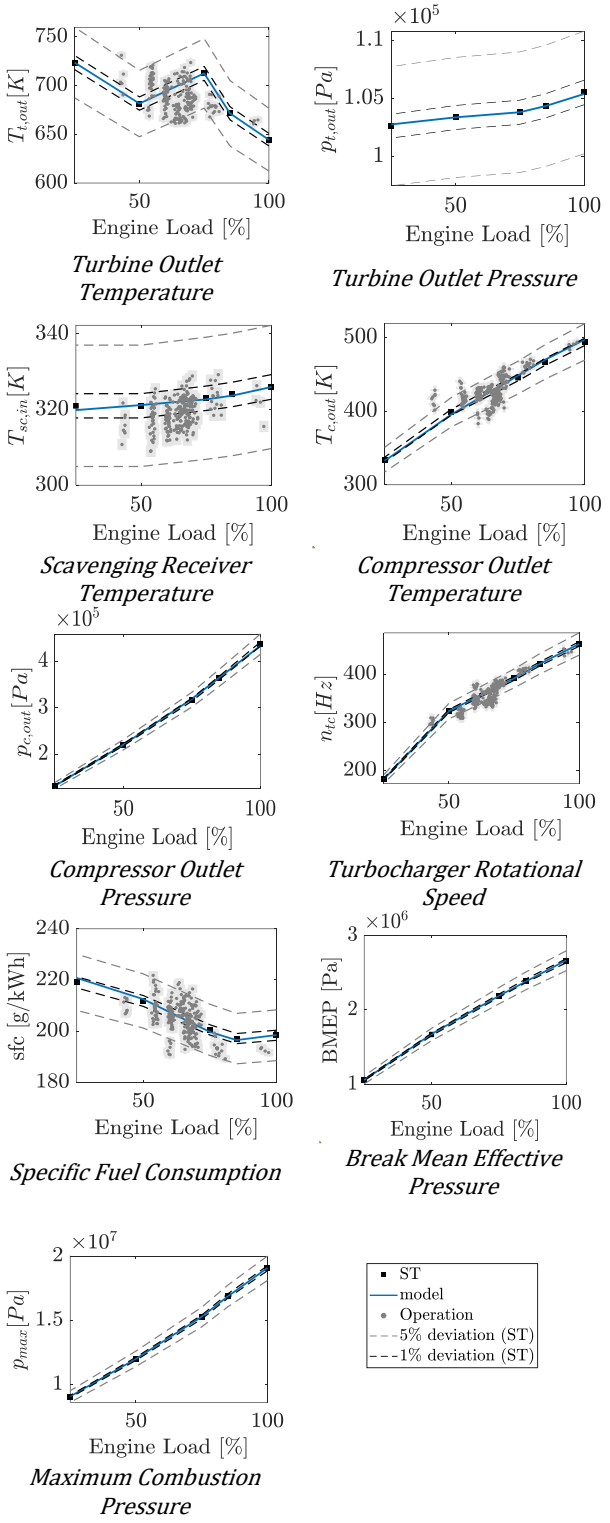

Figure 4. Measurements and model predictions under stationary conditions.

Regarding the validation of the model in stationary conditions, we have to consider the performance on $\mathcal{T}_{\mathcal{K}}$, which contains a set of measurements that are close to the data of $\mathcal{D}_{\mathcal{M}}$, as they are extracted during normal operation of the engine during sailing. Unfortunately, a holistic comparison with the performance on $\mathcal{D}_{\mathcal{M}}$ is not possible, as a subset of signals is available for validation.

Nevertheless, the metrics on Table 5 reveal that a non-negligible discrepancy in performance is present. This discrepancy is expected, since $\mathcal{T}_{\mathcal{K}}$ has not been utilised to calibrate the model and given the internal feedback systems and flow of variables between the control volumes and flow elements according to Section 2.8, all modelling errors are coupled to the rest of the model and amplified.

More specifically, the MAPE on the compressor outlet temperature has increased from 0.638% (2.75 K) on $\mathcal{D}_{\mathcal{M}}$, to 2.752% on $\mathcal{T}_{\mathcal{K}}$. Similarly, the scavenging manifold and turbine outlet temperatures have increased from 0.122% (0.393 K) and 0.01% (0.066 K) to 1.2% (3.8 K) and 2.6% (17.5 K), respectively. It is safe to state that, although pressure measurements are not available on $\mathcal{T}_{\mathcal{K}}$, the relative performance difference of the model between the two datasets would follow a similar trend. Moreover, a similar decrease in prediction capability can be observed for the specific fuel consumption and turbocharger rotational speed, with the MAPEs increasing from 0.041% and 0.056% on $\mathcal{D}_{\mathcal{M}}$, to 3.5% and 2.2%, respectively on $\mathcal{T}_{\mathcal{K}}$.

Table 5. Performance metrics on $\mathcal{T}_{\mathcal{K}}$.

Signal	Units	MAE	MAPE	PPMCC
$T_{c,out}$	K	11.545	2.752	0.643
$T_{sc,in}$	K	3.7980	1.199	0.342
$T_{t,out}$	K	17.545	2.570	-0.145
n_{tc}	Hz	12.013	3.506	0.881
sfc	g/kWh	4.4000	2.178	0.514

Furthermore, Figure 5 reveals that the error range is highest for $T_{c,out}$ and n_{tc} and reach values by as much as 10%, whereas the error range for all other measured signals lies between ± 5%.

This discrepancy in the performance of the model can be explained by a variety of factors: Regarding the temperatures, the differences can be compensated for by the measurement uncertainties of Table 3, which equals 1.5% for all temperature sensors, and an additional 1% maximum approximation error on the estimation of the load of the engine. Regarding sfc and n_{tc}, the variations observed can be attributed to the combined effects of measurement uncertainty, and the lack of knowledge regarding ambient conditions and the exact fuel composition. More specifically, if this information was known, ISO corrections should have been performed for the specific fuel consumption according to the manufacturer documentation, as well as reference correction factors based on the inflow conditions of the working medium on the compressor and turbine. Although we cannot safely estimate the performance increase that these corrections would result in, we expect that if applied, the difference in the predictive performance between $\mathcal{D}_{\mathcal{M}}$ and $\mathcal{T}_{\mathcal{K}}$ would be lower. Figure 6 gives a quantitative view regarding the predictive capabilities in transient conditions. More specifically, the simulated and actual response of the engine are compared during an acceleration and deceleration manoeuvre.

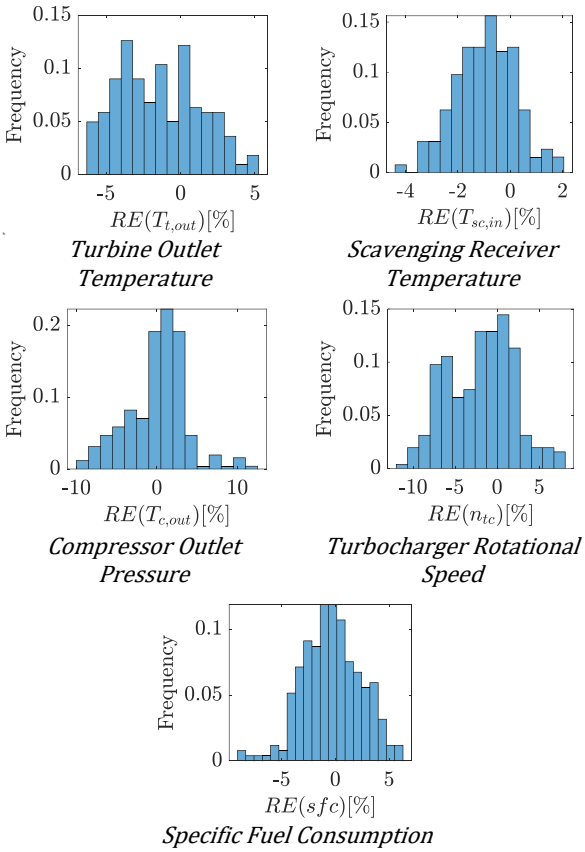

Figure 5. Distribution of absolute percentage errors on $\mathcal{T}_{\mathcal{K}}$.

The engine initially operates at a relatively low load equal to 40%, and a rotational speed of 11.5 Hz, which corresponds to 70% of the rated speed. An acceleration manoeuvre is initiated at approximately 50 seconds, with the engine speed increasing to its nominal value, which subsequently remains constant for a total of 300 seconds. At the same time, the load increases momentarily to the nominal power output, and subsequently it is lowered to 65% at approximately 200 seconds, after which it also remains constant until 350 seconds. Soon after, a deceleration manoeuvre begins, with the engine speed and load reducing to approximately 12 Hz and 40%, respectively.

Overall, the model shows good agreement with the measured data for all signals. The transient response of $T_{c,out}$ is predicted with a maximum error of 4% for the entire simulation, with low stationary errors which for high loads lie within the sensor accuracy. At low loads however, a stationary error of around 3% is present, with a slightly slower response during the deceleration manoeuvre, compared to the measurements. Similar behavior is observed for $T_{t,out}$, which is also over-predicted by around 2%, with a relatively slower response during acceleration. $T_{sc,in}$ is predicted well within the sensor accuracy, although a small constant over-prediction of the signal is present. The response of n_{tc} and power output of the engine (P) are equally well predicted, with

the simulated response varying between ± 2% on average, despite the highly fluctuating recorded values.

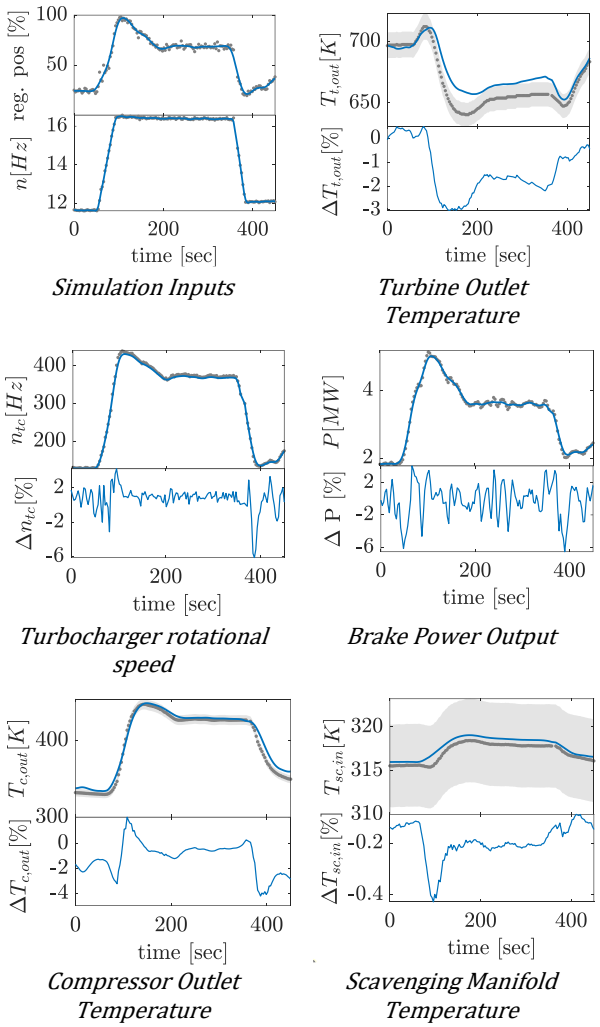

Figure 6. Measurements and model predictions under transient conditions.

6 CONCLUSIONS

A 0-D model for a medium speed DE is described and validated against measured data of a real engine operating in a sailing Roll-on / Roll-off vessel. The automatic calibration processes for stationary and transient operations can provide suitable parameter values to adjust the model's response to the measured signals. The model is shown to capture the stationary engine operation of the engine for a wide span of engine loads, ranging between 20% to 100%.

The stationary relative errors are in general below 3.5\% for the validation data, despite the lack of information regarding the environmental conditions and fuel composition, which is an indication of adequate model accuracy. The dynamic validation of the model shows that it can follow the measured engine signals during transients as well, although the transient responses of the model can be slightly slower than the measured signals.

REFERENCES

[1] C. Garcia-Martos, J. Rodriguez, and M. J. Sanchez. Modelling and forecasting fossil fuels, CO_2 and electricity prices and their volatilities. Applied Energy, 101:363-375, 2013.

[2] Marine Environment Protection Committee. Resolution mepc. 203 (62); amendments to the annex of the protocol of 1997 to amend the international convention for the prevention of pollution from ships, 1973, as modified by the protocol of 1978 relating thereto, 2011.

[3] European Commission. Proposal for a regulation of the european parliament and of the council on the monitoring, reporting and verification of carbon dioxide emissions from maritime transport and amending regulation (eu) n° 525/2013, 2013.

[4] European Commission. Integrating maritime transport in the eu's greenhouse gas reduction policies: Communication from the commission to the european parliament, the council, the european economic and social committee and the committee of the regions, 2013.

[5] H. Lindstad, R. Verbeek, M. Blok, S. van Zyl, A. Hubscher, H. Kramer, J. Purwanto, O. Ivanova, and H. Boonman. Ghg emission reduction potential of eu-related maritime transport and its impacts. Van Mourik Broekmanweg: Delft, The Netherlands, 2015.

[6] F. Tillig, W. Mao, and J. Ringsberg. Systems modelling for energy-efficient shipping. Technical report, Chalmers University of Technology, 2015.

[7] E. A. Bouman, E. Lindstad, A. I. Rialland, and A. H. Strmman. State-of-the-art technologies, measures, and potential for reducing ghg emissions from shipping: a review. Transportation Research Part D: Transport and Environment, 52:408-421, 2017.

[8] A. Miola, M. Marra, and B. Ciu. Designing a climate change policy for the international maritime transport sector: market-based measures and technological options for global and regional policy actions. Energy Policy, 39(9):5490-5498, 2011.

[9] H. Lindstad and G. S. Eskeland. Low carbon maritime transport: How speed, size and slenderness amounts to substantial capital energy substitution. Transportation Research Part D: Transport and Environment, 41:244-256, 2015.

[10] M. Gucwa and A. Schafer. The impact of scale on energy intensity in freight transportation. Transportation Research Part D: Transport and Environment, 23:41-49, 2013.

[11] H.N. Psaraftis and C.A. Kontovas. Ship speed optimization: Concepts, models and combined speed-routing scenarios. Transportation Research Part C: Emerging Technologies, 44:52-69, 2014.

[12] M. Wen, D. Pacino, C.A. Kontovas, and H.N. Psaraftis. A multiple ship routing and speed optimization problem under time, cost and environmental objectives. Transportation Research Part D: Transport and Environment, 52:303-321, 2017.

[13] F. Baldi, H. Johnson, C. Gabrielii, and K. Andersson. Energy and exergy analysis of ship energy systems-the case study of a chemical tanker. In 27th ECOS, International Conference on Efficiency, Cost, Optimization, Simulation and Environmental Impact of Energy Systems, 2014.

[14] F. Baldi, G. Theotokatos, and K. Andersson. Development of a combined mean value - zero dimensional model and application for a large marine four-stroke diesel engine simulation. Applied Energy, 154:402-415, 2015.

[15] S. Lion, I. Vlaskos, and R. Taccani. A review of emissions reduction technologies for low and medium speed marine diesel engines and their potential for waste heat recovery. Energy Conversion and Management, 207:112553, 2020.

[16] K. Kamal and C. Hui. A semi-experimental modeling approach for a large two-stroke marine diesel engine simulation. In 27th CIMAC World Congress, Shanghai, China, 2013.

[17] D. N. Malkhede, B. Seth, and H.C. Dhariwal. Mean value model and control of a marine turbocharged diesel engine. Technical report, SAE Technical Paper, 2005.

[18] C. Guan, G. Theotokatos, P. Zhou, and H. Chen. Computational investigation of a large containership propulsion engine operation at slow steaming conditions. Applied Energy, 130:370-383, 2014.

[19] G. Theotokatos. On the cycle mean value modelling of a large two-stroke marine diesel engine. Proceedings of the Institution of Mechanical Engineers, Part M: Journal of engineering for the maritime environment, 224(3):193-205, 2010.

[20] H. Grimmelius, E.J. Boonen, H. Nicolai, and D. Stapersma. The integration of mean value first principle diesel engine models in dynamic waste heat and cooling load analysis. In CIMAC Congress, Bergen, Norway, volume 31, page 51, 2010.

[21] G. Theotokatos. Ship propulsion plant transient response investigation using a mean value engine model. Int. J. Energy, 2(4):66-74, 2008.

[22] K. Nikzadfar and A.H. Shamekhi. An extended mean value model (emvm) for control-oriented modeling of diesel engines transient performance and emissions. Fuel, 154:275-292, 2015.

[23] R.D. Geertsma, R.R. Negenborn, K. Visser, M.A. Loonstijn, and J.J. Hopman. Pitch control for ships with diesel mechanical and hybrid propulsion: Modelling, validation and performance quantification. Applied Energy, 206:1609-1631, 2017.

[24] G. Theotokatos, C. Guan, H. Chen, and I. Lazakis. Development of an extended mean value engine model for predicting the marine two-stroke engine operation at varying settings. Energy, 143:533-545, 2018.

[25] L. Xiang, G. Theotokatos, and Y. Ding. Investigation on gaseous fuels interchangeability with an extended zero-dimensional engine model. Energy Conversion and Management, 183:500-514, 2019.

[26] F. Mohammadkhani, M. Yari, and F. Ranjbar. A zero-dimensional model for simulation of a diesel engine and exergo-economic analysis of waste heat recovery from its exhaust and coolant employing a high-temperature kalina cycle. Energy Conversion and Management, 198:111782, 2019.

[27] H. Sapra, M. Godjevac, P. De Vos, W. Van Sluijs, Y. Linden, and K. Visser. Hydrogen natural gas combustion in a marine lean-burn si engine: A comparative analysis of seiliger and double wiebe function-based zero-dimensional modelling. Energy Conversion and Management, 207:112494, 2020.

[28] A.E. Catania, R. Finesso, and E. Spessa. Predictive zero-dimensional combustion model for diesel engine feed-forward control. Energy Conversion and Management, 52(10):3159-3175, 2011.

[29] U. Asad, J. Tjong, and M. Zheng. Exhaust gas recirculation – zero dimensional modelling and characterization for transient diesel combustion control. Energy Conversion and Management, 86:309 - 324, 2014.

[30] R. Finesso and E. Spessa. A real time zero-dimensional diagnostic model for the calculation of in-cylinder temperatures, hrr and nitrogen oxides in diesel engines. Energy Conversion and Management, 79:498 - 510, 2014.

[31] G. Livanos, G. Papalambrou, N.P. Kyrtatos, and A. Christou. Electronic engine control for ice operation of tankers. In Proceedings of the 25th CIMAC world congress on combustion engine technology, Vienna, Austria, pages 21-24, 2007.

[32] Y. Ding, D. Stapersma, H. Knoll, H. Grimmelius, and T. Netherland. Characterising heat release in a diesel engine: A comparison between seiliger process and vibe model. CIMAC International Council on Combustion engines, pages 1-13, 2010.

[33] F. Maroteaux and C. Saad. Combined mean value engine model and crank angle resolved in-cylinder modeling with nox emissions model for real-time diesel engine simulations at high engine speed. Energy, 88:515-527, 2015.

[34] Y. Tang, J. Zhang, H. Gan, B. Jia, and Y. Xia. Development of a real-time two-stroke marine diesel engine model with in-cylinder pressure prediction capability. Applied energy, 194:55-70, 2017.

[35] B.J. McBride, M.J. Zehe, and Gordon S. NASA Glenn coefficients for calculating thermodynamic properties of individual species. National Aeronautics and Space Administration, 2002.

[36] N. Watson and M. Janota. Turbocharging the internal combustion engine. Macmillan International Higher Education, 1982.

[37] J.B. Heywood. Internal combustion engines fundamentals, 1988 ch. 11. McGraw-Hill, New York, 1988.

[38] G.P. Merker, C. Schwarz, G. Stiesch, and F. Otto. Simulating Combustion: Simulation of combustion and pollutant formation for engine development. Springer Science & Business Media, 2005.

[39] X. Llamas and L. Eriksson. Control-oriented modeling of two-stroke diesel engines with exhaust gas recirculation for marine applications. Proceedings of the Institution of Mechanical Engineers, Part M: Journal of Engineering for the Maritime Environment, 233(2):551-574, 2019.

[40] G. Theotokatos and V. Tzelepis. A computational study on the performance and emission parameters mapping of a ship propulsion system. Proceedings of the Institution of Mechanical Engineers, Part M: Journal of Engineering for the Maritime Environment, 229(1):58-76, 2015.

[41] D. Descieux and M. Feidt. One zone thermodynamic model simulation of an ignition compression engine. Applied Thermal Engineering, 27(8-9):1457-1466, 2007.

[42] C.D. Rakopoulos, D.C. Rakopoulos, G.C. Mavropoulos, and E.G. Giakoumis. Experimental and theoretical study of the short-term response temperature transients in the cylinder walls of a diesel engine at various operating conditions. Applied Thermal Engineering, 24(5-6):679-702, 2004.

[43] N. Miyamoto, T. Chikahisa, T. Murayama, and R. Sawyer. Description and analysis of diesel engine rate of combustion and performance using wiebe's functions. SAE transactions, 622-633, 1985.

[44] G. Kokkulunk, A. Parlak, and H. Erdem. Determination of performance degradation of a marine diesel engine by using curve based approach. Applied Thermal Engineering, 108:1136-1146, 2016.

[45] G. Sitkei. Uber den dieselmotorischen zundverzug. MTZ, 24(6):190-194, 1963.

[46] T.K. Gogoi and D.C. Baruah. A cycle simulation model for predicting the performance of a diesel engine fuelled by diesel and biodiesel blends. Energy, 35(3):1317-1323, 2010.

[47] G. Woschni and F. Anisits. Eine methode zur vorausberechnung der anderung des brennverlaufs mittelschnellaufender dieselmotoren bei geaenderten betriebsbedingungen. TMZ, 1973.

[48] G.Woschni. A universally applicable equation for the instantaneous heat transfer coefficient in the internal combustion engine. SAE transactions, pages 3065-3083, 1968.

[49] S. Chen and P Flynn. Development of a single cylinder compression ignition research engine. Technical report, SAE Technical Paper, 1965.
[50] C.D. Rakopoulos, D.T. Hountalas, E.I. Tzanos, and G.N. Taklis. A fast algorithm for calculating the composition of diesel combustion products using 11 species chemical equilibrium scheme. Advances in Engineering Software, 19(2):109-119, 1994.
[51] R.K. Hanson and S. Salimian. Survey of rate constants in the n/h/o system. Combustion chemistry, pages 361-421, 1984.
[52] J. Wahlstrom and L. Eriksson. Modelling diesel engines with a variable-geometry turbocharger and exhaust gas recirculation by optimization of model parameters for capturing non-linear system dynamics. Proceedings of the Institution of Mechanical Engineers, Part D: Journal of Automobile Engineering, 225(7):960-986, 2011.
[53] A.R. Conn, K. Scheinberg, and L.N. Vicente. Introduction to derivative-free optimization. SIAM, 2009.
[54] P. Galinier, J.P. Hamiez, J.K. Hao, and D. Porumbel. Handbook of optimization. Springer, 2013.
[55] C.A. Floudas and P. Pardalos. Encyclopedia of optimization. Springer Science & Business Media, 2008.
[56] C. Audet and J.E Dennis. Mesh adaptive direct search algorithms for constrained optimization. SIAM Journal on optimization, 17(1):188-217, 2006.
[57] C. Audet, A.L. Custodio, and J.E. Dennis. Erratum: Mesh adaptive direct search algorithms for constrained optimization. SIAM Journal on Optimization, 18(4):1501-1503, 2008.
[58] V. Torczon. On the convergence of pattern search algorithms. SIAM Journal on optimization, 7(1):1-25, 1997.
[59] R.M. Lewis, V. Torczon, and M.W. Trosset. Direct search methods: then and now. Journal of computational and Applied Mathematics, 124(1-2):191-207, 2000.
[60] A. Coraddu, L. Oneto, F. Baldi, and D. Anguita. Vessels fuel consumption forecast and trim optimisation: a data analytics perspective. Ocean Engineering, 130:351-370, 2017.